Loss of Epidermal HIF-1α Blocks UVB-Induced Tumorigenesis by Affecting DNA Repair Capacity and Oxidative Stress

Walid Mahfouf, Mohsen Hosseini, Elodie Muzotte, Martin Serrano-Sanchez, Lea Dousset, François Moisan, Walid Rachidi, Alain Taieb, Jana Rudolf, Hamid Reza Rezvani

Loss of epidermal hypoxia-inducible factor-1α blocks UVB-induced tumorigenesis by affecting DNA repair capacity and oxidative stress

Walid Mahfouf (https://orcid.org/0000-0002-4113-0384)[1,§], Mohsen Hosseini (https://orcid.org/0000-0002-1686-8512)[1,§], Elodie Muzotte(https://orcid.org/0000-0002-1721-940X)[1,§], Martin Serrano-Sanchez (https://orcid.org/0000-0002-5165-7593)[1], Lea Dousset (https://orcid.org/0000-0002-5332-5736)[1], François Moisan (https://orcid.org/0000-0003-2680-7497)[1], Walid Rachidi (https://orcid.org/0000-0002-0829-7799)[4], Alain Taieb (https://orcid.org/0000-0002-0928-8608) [1,2,3], Jana Rudolf (https://orcid.org/0000-0003-1134-2340)[1], Hamid Reza Rezvani (https://orcid.org/0000-0001-8067-1338)[1,2,*]

1-Univ. Bordeaux, Inserm, BMGIC, U1035, F-33000 Bordeaux, France

2- Centre de Référence pour les Maladies Rares de la Peau, CHU de Bordeaux, France

3- Département de Dermatologie & Dermatologie Pédiatrique, CHU de Bordeaux, France

4- Nucleic Acids Lesions Laboratory, SCIB/INAC, CEA, Université Joseph Fourier-Grenoble, France

Running title: **Pro-carcinogenic role of HIF-1α in UVB-induced tumorigenesis**

§ These authors contributed equally to this work

*** Corresponding Author**

INSERM U1035, Bordeaux, F-33000 France

Email address: hamid-reza.rezvani@u-bordeaux.fr

Phone: +33-557-575-683

Fax: +33-557-571-374

Abstract

Hypoxia-inducible factor-1α (HIF-1α) is constitutively expressed in mouse and human epidermis. It plays a crucial role in skin physiology including the response of keratinocytes to ultraviolet (UV) radiation. However, little information is available about its role in photocarcinogenesis. Using a multistage model of UVB radiation-induced skin cancer, we show that the knockout of *Hif*-1α in the epidermis prevents tumorigenesis, but at the same time triggers the formation of hyperkeratotic plaques. Our results indicate that the absence of oncogenic transformation in *Hif*-1*α*-ablated mice is related to increased DNA repair in keratinocytes, while the formation of hyperkeratotic plaques is caused by an increase in the levels of reactive oxygen species. Indeed, impairing the DNA repair machinery by ablating xeroderma pigmentosum C restored the UVB-induced neoplastic transformation of *Hif*-1α-ablated keratinocytes, while the development of hyperkeratotic plaques was blocked by chronic antioxidant treatment. We conclude that HIF-1α plays a pro-carcinogenic role in UVB-induced tumorigenesis.

Keywords: HIF-1α, hypoxia-inducible factor, ROS, skin cancer, DNA repair, ageing, UVB, squamous cell carcinoma, SCC

Introduction

Hypoxia inducible factor (HIF) 1 is a heterodimeric transcription factor consisting of alpha and beta subunits. The beta subunit is constitutively expressed, while the expression of the alpha subunit is regulated by the relative concentration of oxygen in tissues. Under normoxia, hydroxylation and ubiquitination targets the alpha subunit for proteasomal degradation (Ivan et al., 2001). Reduced activity of prolyl hydroxylases under hypoxic condition results in the stabilization and accumulation of HIF-1α. Upon stabilization and translocation to the nucleus, HIF-1α unites with the beta subunit to bind to the hypoxia-responsive elements of target genes (Kim et al., 2016, Kuschel et al., 2012). HIF-1α is a pivotal player in many biological processes by affecting the expression of hundreds of genes involved in angiogenesis, cell growth and apoptosis, cell adhesion and migration, the energy metabolism and DNA repair (Rezvani et al., 2011a). Therefore, it is not surprising that elevated levels of HIF-1α are generally linked to a poor cancer prognosis. However, a tumor suppressor role for HIF-1α has also been found in some tumors (Gordan et al., 2007, Savai et al., 2005).

Due to a lack of vascularization, the epidermis presents a mildly hypoxic microenvironment and therefore contains relatively high levels of HIF-1α, especially in the basal layer (Rezvani et al., 2011a, Stücker et al., 2002). Epidermal HIF-1α has been shown to play an important role in the skin, especially in local and systemic adaptation to environmental stresses (Rezvani et al., 2011a). We and others have shown that HIF-1α expression is modulated in a biphasic manner by acute UVB exposure (Rezvani et al., 2007, Wunderlich et al., 2008) and that HIF-1α plays an important role in the regulation of keratinocyte responses to UVB (Nys et al., 2010, Rezvani et al., 2007, Turchi et al., 2008). The most frequent lesions arising from UVB exposure are cyclobutane pyrimidine dimers (CPDs) and pyrimidine (6-4) pyrimidone photoproducts (6-4PPs). UVB-induced DNA damage elicits several cellular responses coordinated by components of the DNA damage response (DDR) network. For example, cell

cycle arrest is triggered immediately after UVB exposure, allowing time for damage surveillance and repair (Obacz et al., 2013). Depending on the extent of the DNA damage there are three main scenarios: (i) if the number of lesions is low, they are repaired and the cell cycle restarted; (ii) if there are many lesions, cells may become apoptotic, causing an increase in cell death which is linked to accelerated aging; (iii) if cells are repeatedly damaged, it leads not only to genomic instability and apoptosis but also to an increased mutagenicity rate and the probability of cells becoming cancerous (Marteijn et al., 2014). The repair of UV photoproducts is primarily carried out by the nucleotide excision DNA repair (NER) pathway. Defective NER is associated with several human disorders such as xeroderma pigmentosum (XP). XP type C (XP-C), which arises due to inactivation of the protein XPC, is an autosomal recessive disease characterized by hypersensitivity to UV light, accelerated skin ageing and an increased predisposition to skin cancers (Hosseini et al., 2015a, Hosseini et al., 2015b). Several NER factors (such as XPC, XPD, XPB and XPG) have been shown to be regulated transcriptionally by HIF-1α (Rezvani et al., 2010).

Despite the importance of HIF-1α in skin physiology and pathophysiology, little is known about its role in carcinogenesis induced by chronic UVB exposure. Here, we show that knockout of HIF-1α in the epidermis blocks chronic UVB-induced malignant transformation of keratinocytes by modulating the DDR network and oxidative balance.

Results

The removal of *Hif*-1α from the epidermis leads to more proficient removal of DNA damage after acute UVB irradiation

We previously found that downregulation of HIF-1α in human keratinocytes is accompanied by an increased rate of the removal of UV photoproducts and reduced apoptosis (Rezvani et al., 2007, Rezvani et al., 2010). To investigate whether HIF-1α plays the same role in murine epidermis, a mouse model of inducible *Hif*-1α knockout targeted to keratinocytes (K14-Cre-ER^{T2}/*Hif*-$1\alpha^{flox/flox}$) was used. *Hif*-1α was ablated by topical application of 4-hydroxy-tamoxifen (OHT) to the skin, hereinafter called K-*Hif*-$1^{-/-}$. As controls, we used tamoxifen-treated K14-Cre-ER^{T2} mice, hereinafter referred to as K-*Hif*-$1^{+/+}$. The knockout of *Hif*-1α in keratinocytes did not affect the overall health of the animals (data not shown) or caused any histological abnormalities (**Figure 1a**). Dorsal areas of mice were irradiated with a single dose of UVB and skin biopsies were analyzed for DNA repair capacity (**Figure 1a-d**). Immunohistochemistry (**Figure 1a**), immuno-dot blot analysis (**Figure 1b**) and quantification of CPDs and 6-4PP by HPLC-MS/MS analysis (**Figure 1c**) revealed an increased repair rate of photoproducts in K-*Hif*-$1^{-/-}$ keratinocytes compared with K-*Hif*-$1^{+/+}$ samples. Measurement of CPD removal capacity of K-*Hif*-$1^{+/+}$ skin samples at different time points after UVB irradiation revealed that there was a gradual increase in CPD repair capacity which peaked at 48h. On the contrary, when K-HIF-$1^{-/-}$ mice were irradiated, there was a rapid increase in DNA repair capacity with a peak at 10h, followed with a gradual decease (**Figure 1d**). Furthermore, the baseline CPD removal capacity was about 30% higher in K-*Hif*-$1^{-/-}$ skin extracts than in K-*Hif*-$1^{+/+}$ skin samples (**Figure 1d**). Moreover, the phosphorylation levels of DNA repair-associated kinases and transcription factors (p-ATR, p-CHK1, p-ATM, p-CHK2, p-TP53) were downregulated more rapidly in K-*Hif*-$1^{-/-}$ keratinocytes than in K-*Hif*-$1^{+/+}$ mice

(**Figure 1e**). These *in vivo* experiments showed that DNA repair is faster in *Hif*-1α knockouts than in controls.

We then examined whether the upregulation of DNA repair capacity in K-*Hif*-$1^{-/-}$ could be related to the transcriptional regulation of NER factors by HIF-1α as already described (Rezvani et al., 2010). Analysis of *Xpc*, *Xpd* and *Xpb* mRNA expression confirmed that the absence of HIF-1α profoundly affected the mRNA expression profiles of these NER components (**Supplementary Figure S1**).

When looking at apoptotic factors, we found that caspases 3, 8 and 9 were readily activated within 10 hours after UVB exposure in both strains, but activities decreased thereafter more rapidly in K-*Hif*-$1^{-/-}$ mice (**Figure 1f**). The analysis of cell cycle regulators showed that negative cell-cycle regulators such as $p21^{WAF1}$ and $p16^{INK4A}$ were downregulated more quickly after UVB irradiation in K-*Hif*-$1^{-/-}$ than in K-*Hif*-$1^{+/+}$ mice, while cell-cycle promoters, namely Cdc25C, CDK6, cyclin B and D, showed faster upregulation (**Figure 1e**). When quantifying the distribution of cells in different cell cycle phases, there were far fewer cells in the G0/G1-phase in *Hif*-1α knockout mice than in controls 48 hours after irradiation. At the same time, the number of cells in the S-phase was significantly higher in K-*Hif*-$1^{-/-}$ than in K-*Hif*-$1^{+/+}$ mice (**Figure 1g**). Consistently, a greater number of keratinocytes in the epidermal basal layer of the *Hif*-1α knockout specimen stained positive for Ki-67 than in the control samples (**Figure 1h**).

These results indicate that *Hif*-1α ablation in keratinocytes results in increased DNA repair efficiency and down-regulation of apoptosis, suggesting that HIF-1α might play a pro-carcinogenic role in the epidermis.

Knockout of *Hif*-1α in the epidermis prevents UVB-induced tumor development

To examine the effect of *Hif*-1α ablation on UVB-induced carcinogenesis, we used SKH-1 hairless mice as a model, as they closely mimic photocarcinogenesis in humans (Hosseini et al., 2018). To ensure and optimize efficient *Hif*-1α knockout over a prolonged period, we first used a double fluorescent Cre recombinase reporter mouse (mT/mG) (Muzumdar et al., 2007). In this reporter strain, the membrane-targeted Tomato red (mT) is ubiquitously expressed at baseline levels and expression switches to membrane-bound green-fluorescent protein (mG) in cells that have undergone Cre-mediated excision. mTmG mice were subjected to different regimens of topical application of OHT to the skin and irradiated for 4 months (data not shown). Results showed that topical treatment with 60mg.kg^{-1} OHT in sunflower oil for 5 consecutive days followed with one topical treatment every week ensured efficient recombination (**Supplementary Figure S2a**).

K-*Hif*-1$^{+/+}$ and K-*Hif*-1$^{-/-}$ mice showed no obvious anomalies in the absence of UVB irradiation (**Supplementary Figure S2b**). Monitoring K-*Hif*-1$^{+/+}$ mice during chronic UVB irradiation indicated that while none of them had any obvious abnormalities up to week 12 of irradiation, 7 out of 21 mice exhibited at least one actinic keratosis (AK) lesion at 18 weeks (**Figure 2a**). More than 90% of these mice had an average of 13 tumors of variable sizes, exhibiting an exponential increase in size at 25 weeks of irradiation (**Figure 2a-e**). The skin of *Hif*-1α knockout animals also appeared normal up to week 12 of irradiation, but some of them started to develop moderate hyperkeratotic plaques thereafter. Interestingly, at 25 weeks of UVB irradiation, 14 out of 16 K-*Hif*-1$^{-/-}$ mice exhibited severe hyperkeratosis with scaling, while only 25% (4 out of 16) of these mice displayed a limited number of very small tumors (**Supplementary Figure S2b and Figure 2a-e**). Immunohistochemical analysis showed for K-*Hif*-1$^{+/+}$ mice moderately differentiated SCCs with pockets of high proliferation, while *Hif*-

1α knockout skin displayed papillomatous hyperplasia with hyper- and parakeratosis and no dermal invasion (**Supplementary Figure S2b**). Far fewer nuclei stained positive for Ki-67 in K-*Hif*-$1^{-/-}$ mice than in control counterparts.

We next sought to investigate whether the HIF-1α ablation-mediated increase in DNA repair efficiency could explain the observed phenotype in mice. We quantified the relative levels of photodamage in the DNA after 12 weeks of irradiation by immunodot blot and MS/MS HPLC (**Figure 2f, g**). We found a reduction of 1.7- and 5.6-fold in CPDs and 6-4PP, respectively, in epidermal DNA of K-*Hif*-$1^{-/-}$ compared to controls. Next, the DNA repair capacity of skin nuclear extracts was measured by replacing CPDs in a plasmid with fluorescently-labeled nucleotides. The results indicated a 2.2-fold increased removal of CPDs in *Hif*-1α knockout samples (**Figure 2h**).

These data strongly suggest that the absence of tumor formation upon *Hif*-1α ablation could be related to the increased DNA repair capacity in these mice.

The ablation of *Xpc* partially restores neoplastic transformation of *Hif*-1α-ablated keratinocytes induced by chronic UVB irradiation

To further determine whether the absence of UVB-induced tumorigenic transformation of *Hif*-1α-ablated keratinocytes is fully dependent on increased NER efficiency, the K14-Cre-ER^{T2}/*Hif*-$1\alpha^{flox/flox}$ strain was crossed with $XPC^{-/-}$ mice. The histological analysis of skin biopsies of single knockout *Xpc*$^{-/-}$/ K-*Hif*-$1^{+/+}$ and double knockout *Xpc*$^{-/-}$/ K-*Hif*-$1^{-/-}$ animals revealed epidermis with no obvious abnormalities in the absence of UVB (**Supplementary Figure S3**). By 13 weeks of UVB irradiation, more than 60% of mice in both groups had developed at least one AK lesion (**Figure 3a, b**). Of note, *Xpc*$^{-/-}$/ K-*Hif*-$1^{-/-}$ mice still developed severe hyperkeratosis, a feature not seen in the single knockout model (**Figure 3a**).

By week 17, all *Xpc*$^{-/-}$/ K-*Hif*-1$^{+/+}$ and more than 85% of *Xpc*$^{-/-}$/ K-*Hif*-1$^{-/-}$ mice had developed a large number of tumors exhibiting an exponential increase in size (**Figure 3a-d**). Although, the numbers and the combined volumes of all tumors per mouse were higher in *Xpc*$^{-/-}$/K-*Hif*-1$^{+/+}$ mice than in double knockout mice (**Figure 3c-e**), the two strains showed no difference in tumor growth rates **(Figure 3f**). Immunohistochemical analysis of skin biopsies of *Xpc*$^{-/-}$/ K-*Hif*-1$^{+/+}$ mice showed epidermis with poorly differentiated SCC with follicular and desmoplastic features and dermal invasion (**Supplementary Figure S3**). The double knockout mice showed a less severe phenotype with well-differentiated SCC and some follicular and desmoplastic features. Additionally, aggravated papillomatous hyperplasia was evident, accompanied by thick hyperkeratotic plaques and stratum corneum sloughing (**Supplementary Figure S3 and Figure 3a**). Examining the efficiency to remove the UV photoproduct did not show any significant difference between the two groups (**Figure 3g, h**).

These results indicate that neoplastic transformation of *Hif*-1α-ablated keratinocytes is at least partially restored in an NER-deficient context. However, most of the *Xpc*$^{-/-}$/ K-*Hif*-1$^{-/-}$ mice showed an even stronger development of hyperkeratotic plaques (**Figure 3a**) than the K-*Hif*-1$^{-/-}$ mice (**Figure 2a**), suggesting that the development of hyper- and parakeratosis in the event of *Hif*-1α ablation is forcefully dependent on another factor than NER efficiency.

Increased reactive oxygen species (ROS) levels in *Hif*-1α-ablated keratinocytes trigger the formation of hyperkeratotic plaques

We then sought to investigate whether ROS levels might play a role in the observed phenotype in K-*Hif*-1$^{-/-}$ mice for the following reasons: we and others have highlighted the critical role of ROS in the DDR machinery (Hosseini et al., 2015a, Kodama et al., 2013, Park et al., 2014, Raad et al., 2017, Rezvani et al., 2011c, Rezvani et al., 2011d); increased ROS levels are thought to promote skin aging and cellular senescence (Rinnerthaler et al., 2015,

Velarde et al., 2012); the loss of epidermal *Hif*-1α results in accelerated epidermal aging (Rezvani et al., 2011b); and keratinocytes of irradiated K-*Hif*-$1^{-/-}$ mice exhibited a lower proliferation potential than those of K-*Hif*-$1^{+/+}$ (**Figure 4a-c**). Indeed, positive cell cycle regulators were upregulated upon irradiation less strongly in K-*Hif*-$1^{-/-}$ mice than in K-*Hif*-$1^{+/+}$ mice, while there was a marked increase in the expression of negative cell cycle regulators in *Hif*-1α knockout mice as compared to control animals (**Figure 4a**). These results were further validated by data obtained from a colony formation assay in which the number and size of colonies reflected anchorage-independent growth potential of cells. Results revealed a much lower proliferation potential in irradiated K-*Hif*-$1^{-/-}$ keratinocytes than in K-*Hif*-$1^{+/+}$ ones (**Figure 4b, c**).

To investigate the role of ROS, we first measured ROS levels in epidermal cells of mice at 12 weeks of UVB irradiation. They were 1.18-fold higher in K-*Hif*-$1^{-/-}$ cells than in K-*Hif*-$1^{+/+}$ cells (**Figure 4d**). Concordantly, the antioxidant capacities and activities of three important antioxidant enzymes - catalase, Cu/Zn superoxide dismutase (CuZnSOD), and MnSOD - were found to be much lower in K-*Hif*-$1^{-/-}$ skin than in K-*Hif*-$1^{+/+}$ skin (**Figure 4e, f**). These results suggest that K-*Hif*-$1^{-/-}$ mice have to be more sensitive to oxidative stress than wild type mice. To further examine this hypothesis, keratinocyte isolated from mice were subjected to hydrogen peroxide (H_2O_2). Results showed that the increase in total intracellular ROS levels was more pronounced in K-*Hif*-$1^{-/-}$ keratinocytes (**Supplementary Figure S4a**) and subsequently their survival rate was less preserved (**Supplementary Figure S4b**) compared to control cells. Since the NADPH/$NADP^+$ ratio is one of the most important factors that influences the cellular redox balance via affecting different components of antioxidant systems (e.g. catalase activity or GSH/GSSH ratio) (Ying, 2008), we compared the NADPH/$NADP^+$ ratio between K-*Hif*-$1^{+/+}$ and K-*Hif*-$1^{-/-}$ mice skin. Results indicated that HIF-1α knockdown resulted in a marked reduction in this ratio (**Supplementary Figure S4c).**

Since the NADPH/$NADP^+$ ratio is affected by energy metabolism (Ying, 2008) and considering that HIF-1α is known as a key factor in the regulation of metabolism (Semenza, 2013), we questioned whether modified energy metabolism could be the mechanism underlying the sensitivity to oxidative stress in K-*Hif*-$1^{-/-}$. To answer this question, biochemical functional analysis were performed. First, we quantified cellular respiration, which is a major source of ROS production. Results indicated that basal oxygen consumption rate (OCR) was higher in K-*Hif*-$1^{-/-}$ skin than in control skin (**Supplementary Figure S4d**). On the contrary, glucose consumption and lactate production were lowered in the former samples (**Supplementary Figure S4e, f**). These results indicate that HIF-1α ablation results in modification in skin metabolic profile. However, the precise signaling and metabolic pathways connecting HIF-1α knockdown-mediated reprogramming of energy metabolism and modification in redox balance remains to be elucidated.

To further examine the biological relevance of increased ROS level in K-*Hif*-$1^{-/-}$ mice, we then supplemented the drinking water of animals with the antioxidant N-acetylcysteine (NAC, 2g/L) throughout UVB treatment. The antioxidant property of NAC is principally ascribed to its action as a glutathione precursor and/or its rapid interaction with a variety of radical compounds (Samuni et al., 2013). The assessment of the proliferation potential of keratinocytes (**Figure 4a-c**), ROS levels (**Fig 4d**) and antioxidant capacity (**Figure 4e**) revealed no significant difference between NAC-treated K-*Hif*-$1^{-/-}$ and K-*Hif*-$1^{+/+}$ mice. Furthermore, the analysis of biopsies from UVB-irradiated skin showed that NAC supplementation largely blocked the development of hyperkeratotic plaques in *Hif*-1α-ablated mice (**Figure 4g**). Moreover, this treatment resulted in the formation of tumors in K-*Hif*-$1\alpha^{-/-}$ mice, although at a lower rate than in K-*Hif*-$1\alpha^{+/+}$ mice (**Figure 4g, h**).

These results strongly suggest that the lack of neoplastic transformation of keratinocytes and the formation of hyperkeratotic plaques in *Hif*-1α-ablated mice depend on both NER efficiency and ROS levels.

Successive upregulation of HIF-1α at different stages of carcinogenesis

To investigate what role HIF-1α plays at different stages of skin carcinogenesis, datamining analyses were performed on the two following independent transcriptomic databases: GSE2503 (Nindl et al., 2006) in which human skin specimens were analyzed and compared including 6 healthy, 4 AK and 5 SCC samples; and GSE45216 (Lambert et al., 2014) in which 30 SCC and 16 AK human samples were compared.

Using gene ontology (GO) annotation, we found that the most significantly upregulated biological pathway in SCC was the response to hypoxia (**Figure 5a**). We then performed gene set enrichment analysis (GSEA), which considers groups of genes linked together in functional pathways rather than single transcripts. We used the "Winter_Hypoxia_Up" (M5466) (Winter et al., 2007) enrichment dataset, which includes 126 genes differentially regulated under hypoxia and superimposed it on the GSE2503 and GSE45216 datasets (**Figure 5b**). In other words, we tested whether the set of genes whose activities are linked to hypoxia are enriched in SCC relative to either AK or healthy skin. When using GSE2503 we found that genes involved in the response to hypoxia were significantly enriched in both AK and SCC samples compared to healthy skin, and there was still a stronger enrichment in SCC than in AK ($P << 0.001$). Likewise, GSEA analysis of GSE45216 showed greater enrichment of genes involved in hypoxia in SCC than in AK ($P < 0.01$). In the Nindl cohort, *Hif*-1α mRNA expression levels were markedly elevated in SCC than in either AK or healthy skin

(**Figure 5c**). Similarly, in the Lambert cohort, *Hif*-1α mRNA expression was also greater in SCC than in AK (**Figure 5d**). In line with this, the protein expression of HIF-1α showed progressive upregulation at the different stages of skin carcinogenesis when evaluating skin specimens from healthy individuals, AK, well-, moderately- and poorly-differentiated SCC (**Figure 5e-g**). In agreement with previous findings (Rezvani et al., 2011a), immunostaining of the epidermis of healthy skin showed that HIF-1α was mainly localized in the cytoplasm of cells in the basal layer. However, in AK and in the different stages of SCC, HIF-1α displayed mainly nuclear staining and rather diffuse cytoplasmic staining. Of note, although AK samples showed suprabasal HIF-1α expression, the level was still lower than in basal keratinocytes (**Figure 5e**). Western blotting also revealed the gradual increase in HIF-1α expression during skin carcinogenesis (**Figure 5g**).

These data support the observations we made in our *Hif*-1α knockout model, i.e. that *Hif*-1α is an oncogene that is not only crucial for malignant transformation in response to chronic UVB exposure, but also that it is used by neoplastic cells in growing tumors for their adaption to the microenvironment at all stages of carcinogenesis.

Discussion

In this paper, we show that the deletion of *Hif*-1α in keratinocytes has two profound effects on the skin's responses to chronic UVB exposure: it leads to decreased tumorigenesis by promoting DNA repair efficiency; and it causes skin hyper- and parakeratosis by affecting the redox regulation machinery in keratinocytes.

Epidermal HIF-1α expression is essential for the local and systemic adaptation to a variety of stress conditions including skin maturation, wound healing and ageing (Boutin et al., 2008, Kotch et al., 1999, Rezvani et al., 2011b, Wong et al., 2015). We and others have shown that HIF-1 is also a key effector in the regulation of human keratinocyte responses to UV irradiation-induced damage (Rezvani et al., 2007, Turchi et al., 2008, Wunderlich et al., 2008). In particular, one of the direct consequences of decreased *Hif*-1α expression is an increase in the removal rate of acute UVB irradiation-induced DNA damage via direct upregulation of several components of the DNA repair machinery such as XPC and XPB (Rezvani et al., 2010 and **supplementary Figure S1**). HIF-1α-dependent transcriptional regulation of numerous NER factors may partly explain why DNA repair was more efficient in the absence of HIF-1α (**Figure 1**). HIF-1α has also been shown to affect the UVB-induced DDR network by modulating cell cycle regulators (e.g. $p21^{WAF1}$ and p53) and pro-apoptotic genes such as Noxa, BNIP3 and TNF-related apoptosis-inducing ligand (TRAIL) (Cho et al., 2008, Nys et al., 2010, Rezvani et al., 2007, Turchi et al., 2008). Consistent with this finding, we show here that ablation of *Hif*-1α in mouse epidermis results in an increased repair rate of UVB-induced photoproducts, decreased UVB-induced apoptosis and an accelerated release of keratinocytes from acute UVB-induced cell cycle arrest (**Figure 1**), suggesting the pro-carcinogenic role of HIF-1α in UVB-induced carcinogenesis.

HIF-1 can play a dual role by either supporting or suppressing tumorigenesis depending on the origin, stage and microenvironment of the tumor. In terms of its pro-carcinogenic role, the

contribution of HIF-1α to tumor progression has been ascribed to several mechanisms including promotion of angiogenesis, modulation of the metabolism, and inhibition of apoptosis (Maxwell et al., 1997, Ryan et al., 2000, Semenza, 2010). Consistent with this scenario, elevated levels of HIF-1α protein in cancer patients are linked to more extensive metastases and poor survival (Masoud and Li, 2015, Semenza, 2010). As a tumor suppressor, HIF-1α has been shown to promote anti-tumorigenic growth by directly inhibiting c-Myc (Gordan et al., 2007, Savai et al., 2005). As a result, cells either enter p21-mediated cell cycle arrest or apoptosis. In addition, direct or indirect interaction of HIF-1α with p53, as well as the induction of proapoptotic target genes such as BINP3, have been proposed as two other mechanisms by which HIF-1α inhibits neoplastic transformation of cells and carcinogenesis (Hammond and Giaccia, 2006, Sowter et al., 2001).

Little attention has been given to the role of HIF-1α in cutaneous SCC. The evaluation of *HIF*-1α expression at different stages of SCC genesis in human skin biopsies indicated the continuous upregulation of HIF-1α (**Figure 5e-g**), which is consistent with previous reports of the overexpression of HIF-1α in cutaneous SCC (An et al., 2014, Elson et al., 2000, Seleit et al., 2017). Scortegagna *et al.* (Scortegagna et al., 2009) demonstrated that HIF-1α acted as a tumor suppressor in a transgenic mouse model expressing a stabilized form in keratinocytes. In that study, transgenic mice developed an increased number of papillomas. However, their malignant transformation to SCCs was largely inhibited.

Apart from inflicting DNA damage, UVB radiation can increase intracellular ROS via several pathways, including damage to mitochondrial DNA, upregulation of NADPH oxidases (NOX) and rewiring of the cellular energy metabolism (Rudolf et al., 2018). Our results show that the absence of HIF-1α in keratinocytes is linked to overloading of epidermal cells with UVB-induced oxidative stress (**Figure 4d-f**). This disturbance of the epidermal redox balance resulted eventually in the formation of hyperkeratotic plaques in K-*Hif*-$1^{-/-}$ mice. Furthermore,

the increase in hyperkeratosis seen in *Xpc*$^{-/-}$/ K-*Hif*-1$^{-/-}$ mice (**Figure 3**) might be attributed to additional ROS generated in the absence of functional NER (Rezvani et al., 2011c) and/or the protective role of XPC against oxidative DNA damage via affecting the key base-excision repair (BER) enzymes and/or catalase activity (reviewed in Hosseini et al., 2015a). In support of these notions, boosting the antioxidant capacity blocked the development of hyperkeratotic plaques (**Figure 4**). However, since besides antioxidant activities, NAC has been shown to have other properties such as anti-inflammatory activity and modulation of neurotransmitter systems (Samuni et al., 2013, Tardiolo et al., 2018), the results must be interpreted with precaution.

HIF-1α ablation-induced oxidative stress can be explained by the following mechanisms: HIF-1 shifts the balance between glycolysis and mitochondrial metabolism in favor of the former to further reduce the production of ROS by mitochondria (Fukuda et al., 2007, Papandreou et al., 2006, Zhao et al., 2014); HIF-1α-mediated reprogramming of the energy metabolism is associated with modification in NADPH/NADP^{+} ratio which, in its turn, affects the cellular redox balance through different mechanisms (Ying, 2008); HIF-1 is involved in the process of removing damaged mitochondria by autophagy (Zhang et al., 2008). This suggests that in the absence of HIF-1α, recurrent UVB irradiation may cause an increase in ROS by inducing an accumulation of damaged mitochondria, which eventually leads to increased apoptosis and/or senescence.

Together, these findings indicate that HIF-1α is a promising target for both the prevention and treatment of cutaneous SCC.

Materials and methods

Animals and experimental protocol

Mice were obtained from the following sources: SKH-1 hairless mice from Charles River, K14-Cre-ER^{T2} C57BL/6 from the Jackson Laboratory, and *Hif*-1α$^{flox/flox}$ C57BL/6 from Randall S. Johnson (University of Cambridge, UK) (Boutin et al., 2008, Rezvani et al., 2011b). Both the *Hif*-1α$^{flox/flox}$ and the K14-Cre-ER^{T2} strains were bred into the SKH-1 strain and then inbred for 9 generations. Crossing these strains then generated K14-Cre-ER^{T2}/*Hif*-1α$^{flox/flox}$ SKH-1. *Hif*-1α ablation in keratinocytes was verified by PCR assays on skin DNA (**Supplementary Figure S5**).

mT/mG reporter mice (Gt(ROSA)26Sor$^{tm4(ACTB-tdTomato,-EGFP)Luo}$) (Muzumdar et al., 2007) were purchased from the Jackson Laboratory and crossed first with SKH-1 mice for 7 generations and then with K14-CreER^{T2} transgenic SKH-1 mice.

Hairless *Xpc*$^{-/-}$ mice (a generous gift from Niels de Wind, Leiden, The Netherlands) (Cheo et al., 1997) were generated by breeding them into a SKH-1 background (van Oosten et al., 2000). *Xpc*$^{-/-}$/K14-CreER^{T2}/Hif-1$^{flox/flox}$ and *Xpc*$^{-/-}$/K14-CreER^{T2}/Hif-1$^{+/+}$ were produced by inbreeding *Xpc*$^{+/-}$/K14-CreER^{T2}/Hif-1$^{flox/+}$. Mice were bred and maintained in a pathogen-free mouse facility. All mouse experiments were carried out with the approval of Bordeaux University Animal Care and Use Committee. In all experiments female mice were used. Mice were randomly assigned to each group before the start and experiments were performed blinded with respect to genotype and/or treatment.

Statistics

Comparisons between two groups were made using Student's t-test (two tailed) and a p-value <0.05 (*) was considered significant. Comparisons between more than two groups were

calculated with one-way analysis of variance (ANOVA) followed by Bonferroni's multiple comparison tests. To assess the number and the volumes of tumors, a two-way ANOVA analysis of variance test was used followed by Bonferroni's multiple comparison tests. Comparisons of the volumes of tumors between two groups (i.e. boxplots) were calculated with the Mann-Whitney test. A p-value < 0.05 (*) was considered significant.

Acknowledgments

The authors acknowledge the patients 'support group « Les Enfants de La Lune ». They wish to thank P. Costet (University of Bordeaux) for his valuable expertise as well as Vanessa Bergeron and Doriane Bortolotto for technical assistance. H.R.R. gratefully acknowledges support from the Institut National du Cancer ''INCA_6654'', INCa-Canceropole GSO, ''Société Française de Dermatologie'' and ''La Société de Recherche Dermatologique''.

Author contributions

W.M., M.H., E.M., and M.S.S. performed investigation, formal analysis and contributed in methodology, validation, visualization and writing original draft; L.D., F.M. and W.R. performed some investigation; A.T. contributed in conceptualization, supervision, writing-original draft and writing-review and editing, J.R. contributed in investigation, writing original draft, and writing-review and editing; H.R.R. contributed in supervision, conceptualization, formal analysis, visualization funding acquisition, writing-original draft and writing-review and editing; W.M., M.H. and E.M. contributed equally to this work.

Conflict of interest:

None of the authors have any financial interest related to this work.

References

An X, Xu G, Yang L, Wang Y, Li Y, Mchepange UO, et al. Expression of hypoxia-inducible factor-1α, vascular endothelial growth factor and prolyl hydroxylase domain protein 2 in cutaneous squamous cell carcinoma and precursor lesions and their relationship with histological stages and clinical features. J Dermatol 2014;41(1):76-83.

Boutin AT, Weidemann A, Fu Z, Mesropian L, Gradin K, Jamora C, et al. Epidermal sensing of oxygen is essential for systemic hypoxic response. Cell 2008;133(2):223-34.

Cheo DL, Ruven HJ, Meira LB, Hammer RE, Burns DK, Tappe NJ, et al. Characterization of defective nucleotide excision repair in XPC mutant mice. Mutat Res 1997;374(1):1-9.

Cho Y-S, Bae J-M, Chun Y-S, Chung J-H, Jeon Y-K, Kim I-S, et al. HIF-1α controls keratinocyte proliferation by up-regulating p21(WAF1/Cip1). Biochim Biophys Acta (BBA) - Mol Cell Res 2008;1783(2):323-33.

Elson DA, Ryan HE, Snow JW, Johnson R, Arbeit JM. Coordinate up-regulation of hypoxia inducible factor (HIF)-1alpha and HIF-1 target genes during multi-stage epidermal carcinogenesis and wound healing. Cancer Res 2000;60(21):6189-95.

Fukuda R, Zhang H, Kim J-w, Shimoda L, Dang CV, Semenza GL. HIF-1 Regulates Cytochrome Oxidase Subunits to Optimize Efficiency of Respiration in Hypoxic Cells. Cell 2007;129(1):111-22.

Gordan JD, Thompson CB, Simon MC. HIF and c-Myc: sibling rivals for control of cancer cell metabolism and proliferation. Cancer Cell 2007;12(2):108-13.

Hammond EM, Giaccia AJ. Hypoxia-inducible factor-1 and p53: friends, acquaintances, or strangers? Clin Cancer Res 2006;12(17):5007-9.

Hosseini M, Dousset L, Mahfouf W, Serrano-Sanchez M, Redonnet-Vernhet I, Mesli S, et al. Energy Metabolism Rewiring Precedes UVB-Induced Primary Skin Tumor Formation. Cell Rep 2018;23(12):3621-34.

Hosseini M, Ezzedine K, Taieb A, Rezvani HR. Oxidative and energy metabolism as potential clues for clinical heterogeneity in nucleotide excision repair disorders. J Invest Dermatol 2015a;135(2):341-51.

Hosseini M, Mahfouf W, Serrano-Sanchez M, Raad H, Harfouche G, Bonneu M, et al. Premature Skin Aging Features Rescued by Inhibition of NADPH Oxidase Activity in XPC-Deficient Mice. J Invest Dermatol 2015b;135(4):1108-18.

Ivan M, Kondo K, Yang H, Kim W, Valiando J, Ohh M, et al. HIFalpha Targeted for VHL-Mediated Destruction by Proline Hydroxylation: Implications for O2 Sensing. Science 2001;292(5516):464-8.

Kim Y, Nam HJ, Lee J, Park DY, Kim C, Yu YS, et al. Methylation-dependent regulation of HIF-1α stability restricts retinal and tumour angiogenesis. Nat commun 2016;7:10347.

Kodama R, Kato M, Furuta S, Ueno S, Zhang Y, Matsuno K, et al. ROS-generating oxidases Nox1 and Nox4 contribute to oncogenic Ras-induced premature senescence. Genes Cells 2013;18(1):32-41.

Kotch LE, Iyer NV, Laughner E, Semenza GL. Defective Vascularization of HIF-1α-Null Embryos Is Not Associated with VEGF Deficiency but with Mesenchymal Cell Death. Dev Biol 1999;209(2):254-67.

Kuschel A, Simon P, Tug S. Functional regulation of HIF-1α under normoxia--is there more than post-translational regulation? J Cell Physiol 2012;227(2):514-24.

Lambert SR, Mladkova N, Gulati A, Hamoudi R, Purdie K, Cerio R, et al. Key differences identified between actinic keratosis and cutaneous squamous cell carcinoma by transcriptome profiling. Br J Cancer 2014;110(2):520-9.

Marteijn JA, Lans H, Vermeulen W, Hoeijmakers JHJ. Understanding nucleotide excision repair and its roles in cancer and ageing. Nat Rev Mol Cell Biol 2014;15(7):465-81.

Masoud GN, Li W. HIF-1α pathway: role, regulation and intervention for cancer therapy. Acta Pharm Sin B 2015;5(5):378-89.

Maxwell PH, Dachs GU, Gleadle JM, Nicholls LG, Harris AL, Stratford IJ, et al. Hypoxia-inducible factor-1 modulates gene expression in solid tumors and influences both angiogenesis and tumor growth. Proc Natl Acad Sci U S A 1997;94(15):8104-9.

Muzumdar MD, Tasic B, Miyamichi K, Li L, Luo L. A global double-fluorescent Cre reporter mouse. Genesis (New York, NY : 2000) 2007;45(9):593-605.

Nindl I, Dang C, Forschner T, Kuban RJ, Meyer T, Sterry W, et al. Identification of differentially expressed genes in cutaneous squamous cell carcinoma by microarray expression profiling. Mol Cancer 2006;5(1):30.

Nys K, Van Laethem A, Michiels C, Rubio N, Piette JG, Garmyn M, et al. A p38(MAPK)/HIF-1 pathway initiated by UVB irradiation is required to induce Noxa and apoptosis of human keratinocytes. J Invest Dermatol 2010;130(9):2269-76.

Obacz J, Pastorekova S, Vojtesek B, Hrstka R. Cross-talk between HIF and p53 as mediators of molecular responses to physiological and genotoxic stresses. Mol Cancer 2013;12(1):93.

Papandreou I, Cairns RA, Fontana L, Lim AL, Denko NC. HIF-1 mediates adaptation to hypoxia by actively downregulating mitochondrial oxygen consumption. Cell Metab 2006;3(3):187-97.

Park M-T, Kim M-J, Suh Y, Kim R-K, Kim H, Lim E-J, et al. Novel signaling axis for ROS generation during K-Ras-induced cellular transformation. Cell Death Differ 2014;21(8):1185-97.

Raad H, Serrano-Sanchez M, Harfouche G, Mahfouf W, Bortolotto D, Bergeron V, et al. NADPH Oxidase-1 Plays a Key Role in Keratinocyte Responses to UV Radiation and UVB-Induced Skin Carcinogenesis. J Invest Dermatol 2017;137(6):1311-21.

Rezvani HR, Ali N, Nissen LJ, Harfouche G, de Verneuil H, Taieb A, et al. HIF-1α in epidermis: oxygen sensing, cutaneous angiogenesis, cancer, and non-cancer disorders. J Invest Dermatol 2011a;131(9):1793-805.

Rezvani HR, Ali N, Serrano-Sanchez M, Dubus P, Varon C, Ged C, et al. Loss of epidermal hypoxia-inducible factor-1α accelerates epidermal aging and affects re-epithelialization in human and mouse. J Cell Sci 2011b;124(Pt 24):4172-83.

Rezvani HR, Dedieu S, North S, Belloc F, Rossignol R, Letellier T, et al. Hypoxia-inducible factor-1alpha, a key factor in the keratinocyte response to UVB exposure. J Biol Chem 2007;282(22):16413-22.

Rezvani HR, Kim AL, Rossignol R, Ali N, Daly M, Mahfouf W, et al. XPC silencing in normal human keratinocytes triggers metabolic alterations that drive the formation of squamous cell carcinomas. J Clin Invest 2011c;121(1):195-211.

Rezvani HR, Mahfouf W, Ali N, Chemin C, Ged C, Kim AL, et al. Hypoxia-inducible factor-1alpha regulates the expression of nucleotide excision repair proteins in keratinocytes. Nucleic Acids Res 2010;38(3):797-809.

Rezvani HR, Rossignol R, Ali N, Benard G, Tang X, Yang HS, et al. XPC silencing in normal human keratinocytes triggers metabolic alterations through NOX-1 activation-mediated reactive oxygen species. Biochim Biophys Acta 2011d;1807(6):609-19.

Rinnerthaler M, Bischof J, Streubel MK, Trost A, Richter K. Oxidative stress in aging human skin. Biomolecules 2015;5(2):545-89.

Rudolf J, Raad H, Taieb A, Rezvani HR. NADPH Oxidases and Their Roles in Skin Homeostasis and Carcinogenesis. Antioxid Redox Signal 2018;28(13):1238-61.

Ryan HE, Poloni M, McNulty W, Elson D, Gassmann M, Arbeit JM, et al. Hypoxia-inducible factor-1alpha is a positive factor in solid tumor growth. Cancer Res 2000;60(15):4010-5.

Samuni Y, Goldstein S, Dean OM, Berk M. The chemistry and biological activities of N-acetylcysteine. Biochim Biophys Acta 2013;1830(8):4117-29.

Savai R, Schermuly RT, Voswinckel R, Renigunta A, Reichmann B, Eul B, et al. HIF-1α attenuates tumor growth in spite of augmented vascularization in an A549 adenocarcinoma mouse model. Int J Oncol 2005;27(2):393-400.

Scortegagna M, Martin RJ, Kladney RD, Neumann RG, Arbeit JM. Hypoxia-inducible factor-1alpha suppresses squamous carcinogenic progression and epithelial-mesenchymal transition. Cancer Res 2009;69(6):2638-46.

Seleit I, Bakry OA, Al-Sharaky DR, Ragab RAA, Al-Shiemy SA. Evaluation of Hypoxia Inducible Factor-1α and Glucose Transporter-1 Expression in Non Melanoma Skin Cancer: An Immunohistochemical Study. J Clin Diagn Res 2017;11(6):EC09-EC16.

Semenza GL. Defining the role of hypoxia-inducible factor 1 in cancer biology and therapeutics. Oncogene 2010;29(5):625-34.

Semenza GL. HIF-1 mediates metabolic responses to intratumoral hypoxia and oncogenic mutations. J Clin Invest 2013;123(9):3664-71.

Sowter HM, Ratcliffe PJ, Watson P, Greenberg AH, Harris AL. HIF-1-dependent regulation of hypoxic induction of the cell death factors BNIP3 and NIX in human tumors. Cancer Res 2001;61(18):6669-73.

Stücker M, Struk A, Altmeyer P, Herde M, Baumgärtl H, Lübbers DW. The cutaneous uptake of atmospheric oxygen contributes significantly to the oxygen supply of human dermis and epidermis. J Physiol 2002;538(3):985-94.

Tardiolo G, Bramanti P, Mazzon E. Overview on the Effects of N-Acetylcysteine in Neurodegenerative Diseases. Molecules 2018;23(12).

Turchi L, Aberdam E, Mazure N, Pouysségur J, Deckert M, Kitajima S, et al. Hif-2alpha mediates UV-induced apoptosis through a novel ATF3-dependent death pathway. Cell Death Differ 2008;15(9):1472-80.

van Oosten M, Rebel H, Friedberg EC, van Steeg H, van der Horst GT, van Kranen HJ, et al. Differential role of transcription-coupled repair in UVB-induced G2 arrest and apoptosis in mouse epidermis. Proc Natl Acad Sci U S A 2000;97(21):11268-73.

Velarde MC, Flynn JM, Day NU, Melov S, Campisi J. Mitochondrial oxidative stress caused by Sod2 deficiency promotes cellular senescence and aging phenotypes in the skin. Aging 2012;4(1):3-12.

Winter SC, Buffa FM, Silva P, Miller C, Valentine HR, Turley H, et al. Relation of a hypoxia metagene derived from head and neck cancer to prognosis of multiple cancers. Cancer Res 2007;67(7):3441-9.

Wong WJ, Richardson T, Seykora JT, Cotsarelis G, Simon MC. Hypoxia-inducible factors regulate filaggrin expression and epidermal barrier function. J Invest Dermat 2015;135(2):454-61.

Wunderlich L, Paragh G, Wikonkál NM, Bánhegyi G, Kárpáti S, Mandl J. UVB induces a biphasic response of HIF-1alpha in cultured human keratinocytes. Exp Dermatol 2008;17(4):335-42.

Ying W. NAD+/NADH and NADP+/NADPH in cellular functions and cell death: regulation and biological consequences. Antioxid Redox Signal 2008;10(2):179-206.

Zhang H, Bosch-Marce M, Shimoda LA, Tan YS, Baek JH, Wesley JB, et al. Mitochondrial autophagy is an HIF-1-dependent adaptive metabolic response to hypoxia. J Biol Chem 2008;283(16):10892-903.

Zhao T, Zhu Y, Morinibu A, Kobayashi M, Shinomiya K, Itasaka S, et al. HIF-1-mediated metabolic reprogramming reduces ROS levels and facilitates the metastatic colonization of cancers in lungs. Sci Rep 2014;4:3793.

Figures and Figure legends

Figure 1: *Hif*-1 knockout in mouse keratinocytes leads to increased DNA repair efficiency, decreased apoptosis and quicker restart of the cell cycle upon UVB irradiation.

SKH-1 mice were exposed to acute UVB (150 mJ/cm^2) and skin samples harvested at indicated time points post UV-treatment. Control mice (K-*Hif*-1$^{+/+}$) were compared to epidermal conditional *Hif*-1α knockout animals (K-*Hif*-1$^{-/-}$).

(**a, b**) The DNA repair capacity of keratinocytes was assessed by anti-CPD staining of (**a**) skin sections and (**b**) quantified by immuno-dot blot of the respective genomic DNA. SYBR green was used as loading control.

(**c**) The number of CPDs and 6-4PPs was quantified at the indicated time points after irradiation by HPLC-MS/MS.

(**d**) The capacity of CPD excision and the re-synthesis was calculated by adding skin protein extracts on a fixed plasmid harboring a defined quantity of CPD. The capacity of CPD repair is directly correlated with the incorporation of labeled nucleotides. Black * for irradiated skin samples versus non-irradiated samples; Grey * for K-*Hif*-1$^{-/-}$ samples versus K-*Hif*-1$^{+/+}$ at the indicated time points.

(**e**) The presence of cell cycle regulators and the activation of caspase-3 were assessed by Western blot of skin total protein extracts. β-actin was used as loading control.

(**f**) Caspase-3, -8, and -9 activities were measured at indicated times after UVB irradiation. RLU: relative luminescent units.

(**g**) The distribution of cells at G1, S and G2 stages of the cell cycle were measured at the indicated intervals after irradiation.

(**h**) Skin sections were stained for the proliferation marker Ki-67.

N=12 animals/ group (**c, d, e, f, g**) Results are expressed in means +/- SD. Statistical significance: *P≤0.05, ***P≤0.001. Scale bars, 50 µm.

Figure 2: Keratinocyte-specific knockout of *Hif*-1α blocks neoplastic transformation of keratinocytes by affecting DNA repair capacity.

(**a**) Photographs are representative examples of *Hif*-1α knockout mice (K-*Hif*-$1^{-/-}$) and their control counterparts (K-*Hif*-$1^{+/+}$) after 12, 18 and 25 weeks of chronic UVB irradiation. K-*Hif*-$1^{+/+}$ animals exhibit mostly actinic keratoses and tumors, sometimes ulcerated, that varied in number and size. K-*Hif*-$1^{-/-}$ were covered by large psoriasiform hyperkeratotic plaques and some actinic keratoses, but no tumors were detected.

(**b**) The percentage of tumor-free mice was assessed at times indicated.

(**c, d**) The numbers (**c**) and combined volumes (**d**) of tumors/ mouse were recorded at different intervals.

(**e**) The distribution of the mean volume of all single tumors/ mouse is presented at week 25 of chronic UVB irradiation.

(**f, g**) Photoproducts were quantified 12 weeks of chronic UVB irradiation by (**f**) dot blot and (**g**) HPLC-MS/MS.

(**h**) The capacity of CPD excision and DNA re-synthesis is shown as a result of quantification of relative fluorescence intensities.

nIr, non-irradiated; Ir, irradiated. N=21 (K-*Hif*-$1^{+/+}$) and N=16 (K-*Hif*-$1^{-/-}$) for **b-e** and N=10 animals/group for **g-h**. Results are expressed as means +/- SEM for **b-d** and means +/- SD for **g-h**. Statistical significance: **P≤0.01, ***P≤0.001, ****P≤0.0001.

Figure 3. Ablation of *Xpc* in *Hif*-1α knockout mice restores UVB-induced neoplastic transformation in keratinocytes.

(**a**) Photographs are representative examples of double knockout mice (*Xpc*$^{-/-}$/K-*Hif*-1$^{-/-}$) and their control counterparts (*Xpc*$^{-/-}$/K-*Hif*-1$^{+/+}$) after 6, 12 and 17 weeks of chronic UVB irradiation. In addition to keratotic plaques *Xpc*$^{-/-}$/K-*Hif*-1$^{-/-}$mice develop tumors of variable size and numbers.

(**b-d**) The percentage of tumor-free mice (**b**) as well as the number (**c**) and mean volumes of all single tumors per mouse (**d**) were assessed up to 17 weeks post-UVB irradiation.

(**e, f**) The distribution of the combined volumes of all single tumors/ mouse (**e**) and the specific tumor growth rate SRG (**f**) were estimated for each mouse according to the following equation: SRG=Ln2/DT, in which DT= doubling time.

(**g, h**) Photoproducts were quantified at 12 weeks of chronic UVB irradiation by immuno-dot blot (**g**) and HPLC-MS/MS (**h**).

nIr, non-irradiated; Ir, irradiated. N=16 (*Xpc*$^{-/-}$/K-*Hif*-1$^{+/+}$) and N=15 (*Xpc*$^{-/-}$/K-*Hif*-1$^{-/-}$) for **b-e**, and N=10 animals/group for **g-h**. Results are expressed in means +/- SEM for **b-d** and means +/- SD for **h**. Statistical significance: **P≤0.01, ***P≤0.001, ****P≤0.0001.

Figure 4. Antioxidant (NAC) supplementation blocks completely chronic UVB irradiation-induced hyperkeratosis in *Hif*-1α ablated mice

K-*Hif-1*$^{+/+}$ and K-*Hif*$^{-/-}$ mice were subjected to chronic UVB irradiation ± NAC for 25 weeks.

(**a**) Total protein extracts were assessed for cell-cycle regulators by Western blot analysis. β-actin was used as a loading control.

(**b, c**) Assessment of the proliferation potential of keratinocytes by colony-forming efficiency and distribution of colony types of irradiated K-*Hif-1*$^{-/-}$ and K-*Hif-1*$^{+/+}$.

(**d-f**) The relative ROS levels (**d**), the total cellular antioxidant capacity expressed in Trolox^{TM} equivalents (**e**) and catalase, CuZnSOD, and MnSOD activities (**f**) in mouse skin were evaluated.

(**g-j**) NAC-treated K-*Hif-1*$^{-/-}$ and K-*Hif-1*$^{+/+}$ mice were subjected to chronic UVB irradiation (**g**). The number of mice harboring tumors (**h**), the tumor number/ mouse (**i**), and the total volume of all tumors/ mouse (**j**) were assessed (mean ± SEM) at times indicated.

N=6 mice per group for **c** and 13 mice per group for **d-j**. *P< 0.05, **P≤0.01, ***P≤0.001, ****P≤0.0001.

Figure 5. Increase in *HIF*-1α expression during skin carcinogenesis.

(**a**) Enrichment analyses were done on GSE2503 (Nindl et al., 2006) and GSE45216 (Lambert et al., 2014) transcriptomic databases to evaluate the upregulation of biological processes in SCC versus healthy skin and/or AK.

(b) "Winter_Hypoxia_Up" (Winter et al., 2007) gene set taken from GO database (GSEA M5466) was used to test enrichment of the genes involved in response to hypoxia in SCC versus AK and/or healthy skin using GSE2503 and GSE45216 transcriptomic databases.

(c,d) *HIF*-1α mRNA expression in healthy skin, AK and SCC was evaluated in Nindl(Nindl et al., 2006) (**c**) and Lambert (Lambert et al., 2014) (**d**) transcriptomic data bases (GSE2503 and GSE45216).

(**e**) HIF-1α expression was assessed in human skin specimens at different stages of tumorigenesis. Scale bars = 50µm.

(**f**) Graph shows quantification of HIF-1α staining score (0-30 = no to very weak staining to 200-300 = high staining score) of the human skin sections presented in (**e**). The basal layer was excluded from the analysis.

(**g**) Western blot depicting the expression of HIF-1α in human skin specimens at different stages of tumorigenesis. ß-actin was used as a loading control.

Figure 1

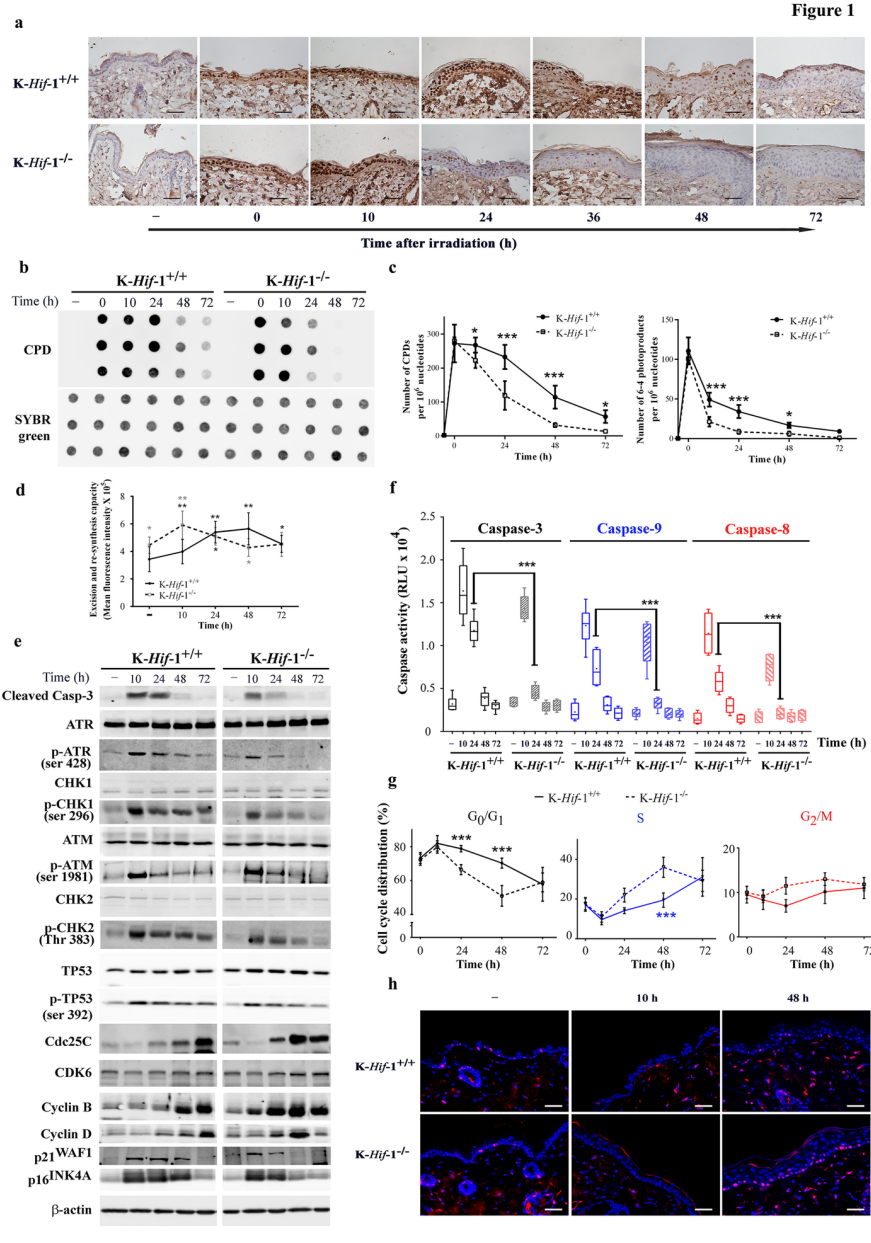
a
K-Hif-1+/+
K-Hif-1-/-
– 0 10 24 36 48 72
Time after irradiation (h)
b
K-Hif-1+/+
K-Hif-1-/-
Time (h)
CPD
SYBR green
c
Number of CPDs per 10^6 nucleotides
Number of 6-4 photoproducts per 10^6 nucleotides
Time (h)
d
Excision and re-synthesis capacity (Mean fluorescence intensity X 10^3)
Time (h)
e
Cleaved Casp-3
ATR
p-ATR (ser 428)
CHK1
p-CHK1 (ser 296)
ATM
p-ATM (ser 1981)
CHK2
p-CHK2 (Thr 383)
TP53
p-TP53 (ser 392)
Cdc25C
CDK6
Cyclin B
Cyclin D
p21WAF1
p16INK4A
β-actin
f
Caspase-3
Caspase-9
Caspase-8
Caspase activity (RLU x 10^4)
Time (h)
g
G0/G1
S
G2/M
Cell cycle distribution (%)
Time (h)
h
–
10 h
48 h

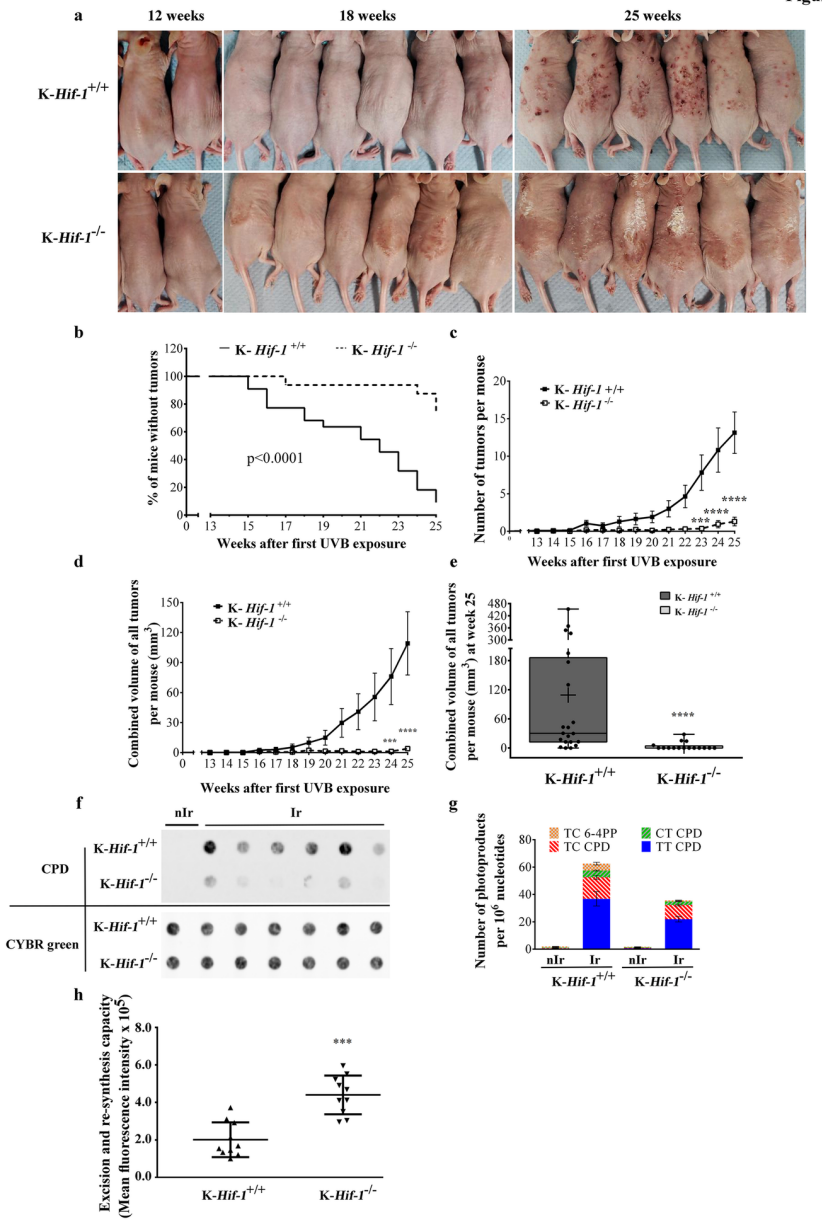
a
12 weeks
18 weeks
25 weeks
K-Hif-1+/+
K-Hif-1-/-
b
K- Hif-1 +/+
K- Hif-1 -/-
% of mice without tumors
p<0.0001
Weeks after first UVB exposure
c
K- Hif-1 +/+
K- Hif-1 -/-
Number of tumors per mouse
Weeks after first UVB exposure
d
K- Hif-1 +/+
K- Hif-1 -/-
Combined volume of all tumors per mouse (mm3)
Weeks after first UVB exposure
e
K- Hif-1 +/+
K- Hif-1 -/-
Combined volume of all tumors per mouse (mm3) at week 25
K-Hif-1+/+
K-Hif-1-/-
f
nIr
Ir
CPD
CYBR green
K-Hif-1+/+
K-Hif-1-/-
g
TC 6-4PP
TC CPD
CT CPD
TT CPD
Number of photoproducts per 10^6 nucleotides
nIr
Ir
K-Hif-1+/+
K-Hif-1-/-
h
Excision and re-synthesis capacity (Mean fluorescence intensity x 10^5)
K-Hif-1+/+
K-Hif-1-/-

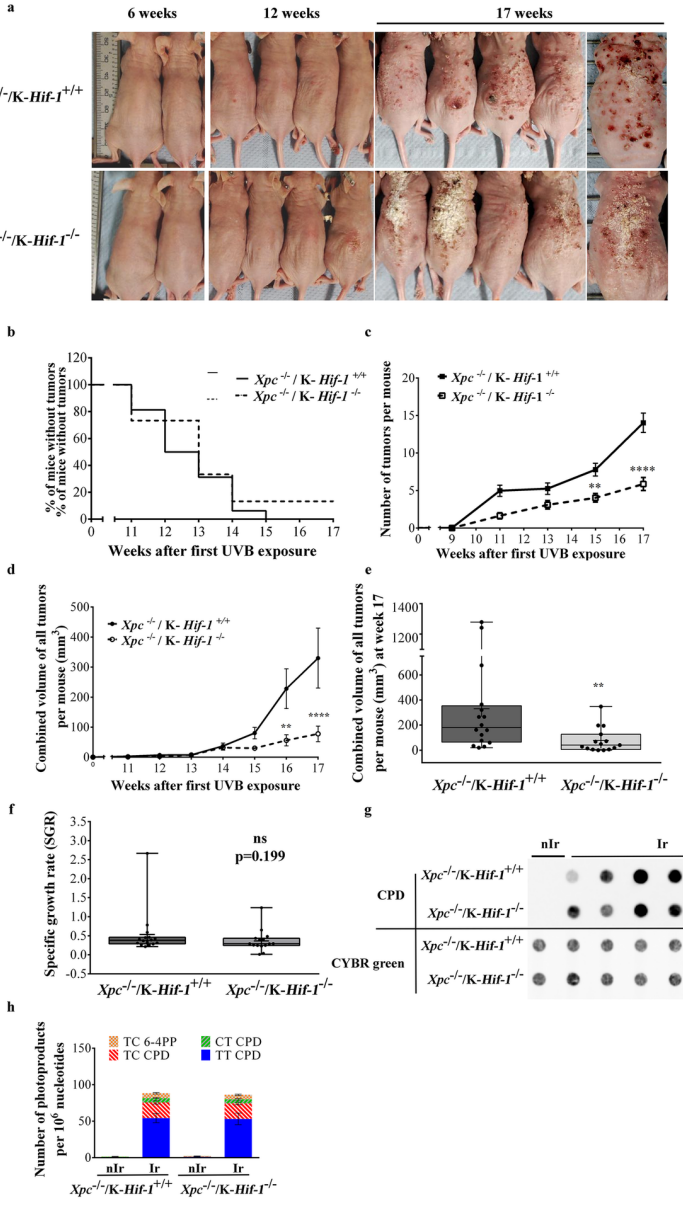
a
6 weeks
12 weeks
17 weeks
Xpc-/-/K-Hif-1+/+
Xpc-/-/K-Hif-1-/-
b
% of mice without tumors
Xpc -/- / K- Hif-1 +/+
Xpc -/- / K- Hif-1 -/-
Weeks after first UVB exposure
c
Number of tumors per mouse
Xpc -/- / K- Hif-1 +/+
Xpc -/- / K- Hif-1 -/-
**
****
Weeks after first UVB exposure
d
Combined volume of all tumors per mouse (mm3)
Xpc -/- / K- Hif-1 +/+
Xpc -/- / K- Hif-1 -/-
**
****
Weeks after first UVB exposure
e
Combined volume of all tumors per mouse (mm3) at week 17
**
Xpc-/-/K-Hif-1+/+
Xpc-/-/K-Hif-1-/-
f
Specific growth rate (SGR)
ns
p=0.199
Xpc-/-/K-Hif-1+/+
Xpc-/-/K-Hif-1-/-
g
nIr
Ir
CPD
CYBR green
Xpc-/-/K-Hif-1+/+
Xpc-/-/K-Hif-1-/-
h
Number of photoproducts per 10^6 nucleotides
TC 6-4PP
TC CPD
CT CPD
TT CPD
nIr
Ir
Xpc-/-/K-Hif-1+/+
Xpc-/-/K-Hif-1-/-

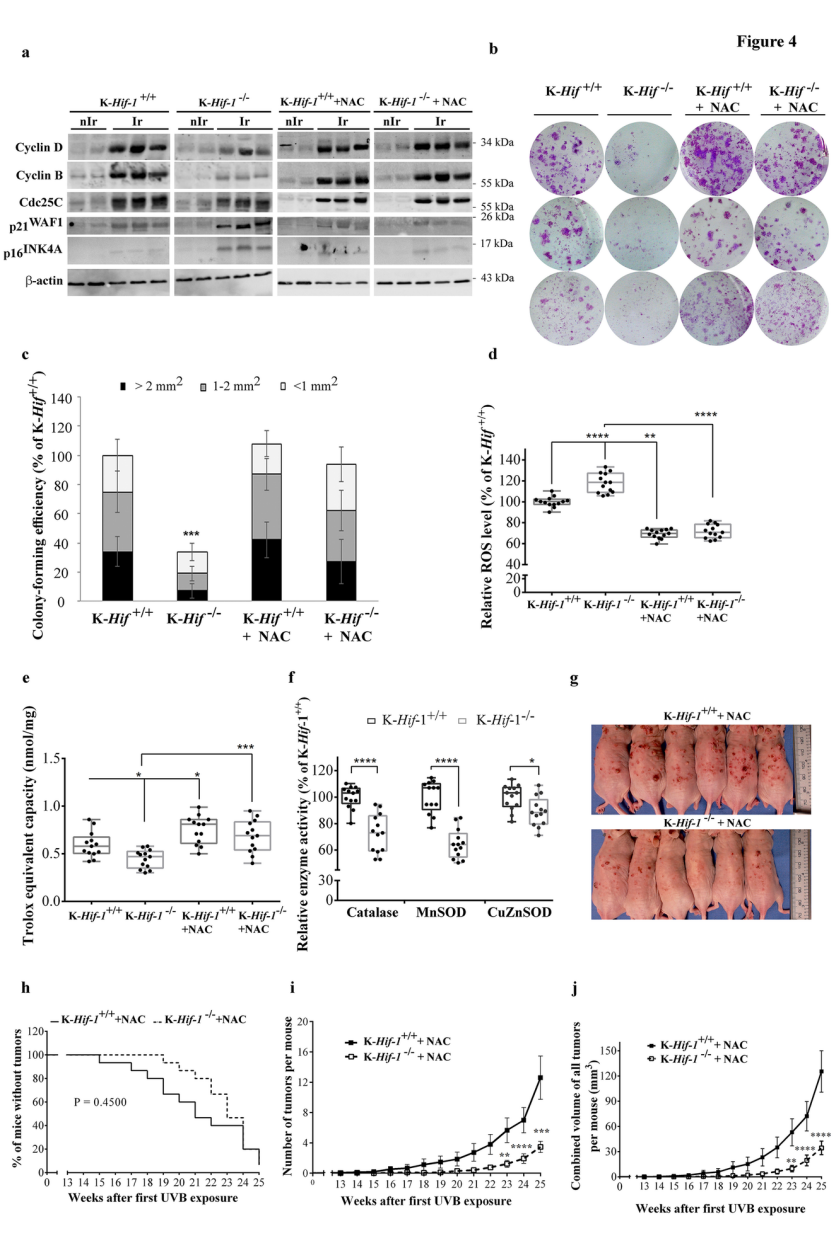
a
K-Hif-1 +/+
K-Hif-1 -/-
K-Hif-1 +/+ +NAC
K-Hif-1 -/- + NAC
nIr
Ir
Cyclin D
Cyclin B
Cdc25C
p21WAF1
p16INK4A
β-actin
34 kDa
55 kDa
55 kDa
26 kDa
17 kDa
43 kDa
b
K-Hif-/+/+
K-Hif-/-
K-Hif-/+/+ + NAC
K-Hif-/-/- + NAC
c
> 2 mm2
1-2 mm2
<1 mm2
Colony-forming efficiency (% of K-Hif-/+/+)
***
K-Hif-/+/+
K-Hif-/-/-
K-Hif-/+/+ + NAC
K-Hif-/-/- + NAC
d
Relative ROS level (% of K-Hif-/+/+)
****
**
****
K-Hif-1+/+
K-Hif-1-/-
K-Hif-1+/+ +NAC
K-Hif-1-/- +NAC
e
Trolox equivalent capacity (nmol/mg)
*
*
***
K-Hif-1+/+
K-Hif-1-/-
K-Hif-1+/+ +NAC
K-Hif-1-/- +NAC
f
K-Hif-1+/+
K-Hif-1-/-
Relative enzyme activity (% of K-Hif-1+/+)
****
****
*
Catalase
MnSOD
CuZnSOD
g
K-Hif-1+/+ + NAC
K-Hif-1-/- + NAC
h
K-Hif-1+/+ +NAC
K-Hif-1-/- +NAC
% of mice without tumors
P = 0.4500
Weeks after first UVB exposure
i
K-Hif-1+/+ + NAC
K-Hif-1-/- + NAC
Number of tumors per mouse
**
****
***
Weeks after first UVB exposure
j
K-Hif-1+/+ + NAC
K-Hif-1-/- + NAC
Combined volume of all tumors per mouse (mm3)
**
****
****
Weeks after first UVB exposure

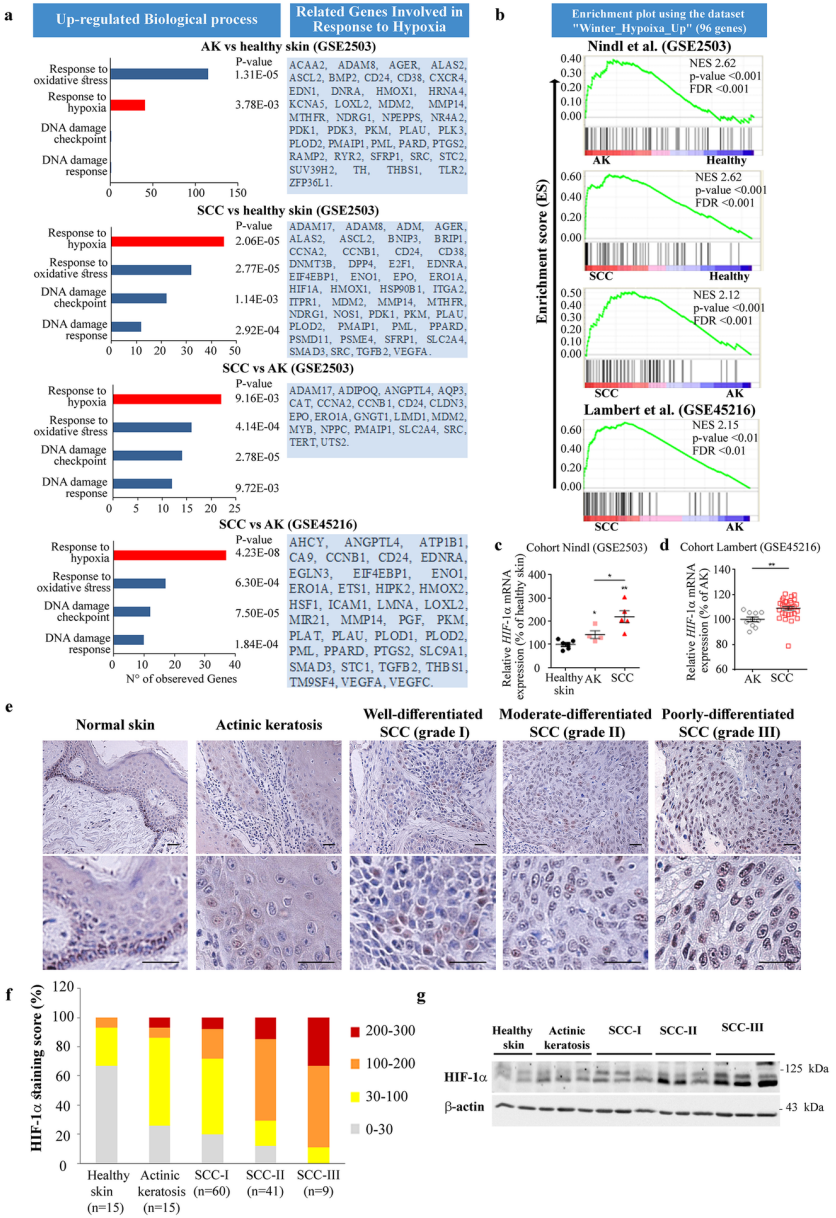
a
Up-regulated Biological process
Related Genes Involved in Response to Hypoxia
AK vs healthy skin (GSE2503)
P-value
Response to oxidative stress
1.31E-05
Response to hypoxia
3.78E-03
DNA damage checkpoint
DNA damage response
0
50
100
150
ACAA2, ADAM8, AGER, ALAS2, ASCL2, BMP2, CD24, CD38, CXCR4, EDN1, DNRA, HMOX1, HRNA4, KCNA5, LOXL2, MDM2, MMP14, MTHFR, NDRG1, NPEPPS, NR4A2, PDK1, PDK3, PKM, PLAU, PLK3, PLOD2, PMAIP1, PML, PARD, PTGS2, RAMP2, RYR2, SFRP1, SRC, STC2, SUV39H2, TH, THBS1, TLR2, ZFP36L1.
SCC vs healthy skin (GSE2503)
P-value
Response to hypoxia
2.06E-05
Response to oxidative stress
2.77E-05
DNA damage checkpoint
1.14E-03
DNA damage response
2.92E-04
0
10
20
30
40
50
ADAM17, ADAM8, ADM, AGER, ALAS2, ASCL2, BNIP3, BRIP1, CCNA2, CCNB1, CD24, CD38, DNMT3B, DPP4, E2F1, EDNRA, EIF4EBP1, ENO1, EPO, ERO1A, HIF1A, HMOX1, HSP90B1, ITGA2, ITPR1, MDM2, MMP14, MTHFR, NDRG1, NOS1, PDK1, PKM, PLAU, PLOD2, PMAIP1, PML, PPARD, PSMD11, PSME4, SFRP1, SLC2A4, SMAD3, SRC, TGFB2, VEGFA.
SCC vs AK (GSE2503)
P-value
Response to hypoxia
9.16E-03
Response to oxidative stress
4.14E-04
DNA damage checkpoint
2.78E-05
DNA damage response
9.72E-03
0
5
10
15
20
25
ADAM17, ADIPOQ, ANGPTL4, AQP3, CAT, CCNA2, CCNB1, CD24, CLDN3, EPO, ERO1A, GNGT1, LMD1, MDM2, MYB, NPPC, PMAIP1, SLC2A4, SRC, TERT, UTS2.
SCC vs AK (GSE45216)
P-value
Response to hypoxia
4.23E-08
Response to oxidative stress
6.30E-04
DNA damage checkpoint
7.50E-05
DNA damage response
1.84E-04
0
10
20
30
40
N° of obsereved Genes
AHCY, ANGPTL4, ATP1B1, CA9, CCNB1, CD24, EDNRA, EGLN3, EIF4EBP1, ENO1, ERO1A, ETS1, HIPK2, HMOX2, HSF1, ICAM1, LMNA, LOXL2, MIR21, MMP14, PGF, PKM, PLAT, PLAU, PLOD1, PLOD2, PML, PPARD, PTGS2, SLC9A1, SMAD3, STC1, TGFB2, THBS1, TM9SF4, VEGFA, VEGFC.
b
Enrichment plot using the dataset "Winter_Hypoixa_Up" (96 genes)
Nindl et al. (GSE2503)
Enrichment score (ES)
NES 2.62
p-value <0.001
FDR <0.001
AK
Healthy
NES 2.62
p-value <0.001
FDR <0.001
SCC
Healthy
NES 2.12
p-value <0.001
FDR <0.001
SCC
AK
Lambert et al. (GSE45216)
NES 2.15
p-value <0.01
FDR <0.01
SCC
AK
c
Cohort Nindl (GSE2503)
Relative HIF-1α mRNA expression (% of healthy skin)
Healthy skin
AK
SCC
d
Cohort Lambert (GSE45216)
Relative HIF-1α mRNA expression (% of AK)
AK
SCC
e
Normal skin
Actinic keratosis
Well-differentiated SCC (grade I)
Moderate-differentiated SCC (grade II)
Poorly-differentiated SCC (grade III)
f
HIF-1α staining score (%)
200-300
100-200
30-100
0-30
Healthy skin (n=15)
Actinic keratosis (n=15)
SCC-I (n=60)
SCC-II (n=41)
SCC-III (n=9)
g
Healthy skin
Actinic keratosis
SCC-I
SCC-II
SCC-III
HIF-1α
125 kDa
β-actin
43 kDa